

The Drell-Yan process as a testing ground for parton distributions up to LHC

Eduardo Basso

Department of Astronomy and Theoretical Physics,
Lund University, SE 223-62 Lund, Sweden

Claude Bourrely

Aix Marseille Université, Université de Toulon, CNRS, CPT, UMR 7332
13288 Marseille, Cedex 09, France

Roman Pasechnik

Department of Astronomy and Theoretical Physics,
Lund University, SE 223-62 Lund, Sweden

Jacques Soffer

Physics Department, Temple University,
1925 N, 12th Street, Philadelphia, PA 19122-1801, USA

Abstract

The Drell-Yan massive dilepton production in hadron-hadron collisions provides a unique tool, complementary to Deep Inelastic Scattering, for improving our understanding of hadronic substructure and in particular for testing parton distributions. We will consider measurements of the differential and double-differential Drell-Yan cross sections from FNAL Tevatron up to CERN LHC energies and they will be compared to the predictions of perturbative QCD calculations using most recent sets (CT14 and MMHT14) of parton distribution functions, as well as those provided by the statistical approach.

Key words: Drell-Yan process, parton distribution functions

PACS numbers: 12.40.Ee, 13.38.Bx, 14.70.Hp

1 Introduction

The Deep Inelastic Scattering (DIS) of leptons and nucleons is indeed our main source of information to study the internal nucleon structure in terms of parton distribution functions (PDF). However at hadron colliders, one has access to the Drell-Yan (DY) process [1] and the measurement of massive dilepton production, via Z/γ^* exchange in the s channel $Z/\gamma^* \rightarrow l\bar{l}$, is also an excellent, unique and clean observable for testing QCD and, in particular, the nucleon structure encoded in PDFs [2]. Needless to mention, the DY process is one of the standard candles for New Physics searches at the energy and luminosity frontiers which thus requires a significant reduction in theoretical uncertainties. This is the reason why several DY experiments were already performed in almost all high-energy hadronic facilities and they are now being intensively studied in all on-going major experiments at the Large Hadron Collider (LHC) at CERN. This will allow us to test various theoretical models in a vast kinematical domain and to analyse the corresponding PDF uncertainties with this simple process whose mechanism is dominated by parton-antiparton annihilation in pp collisions.

The rapidity y and the invariant mass $M_{l\bar{l}}$ of the dilepton system produced in proton-proton collisions are related, at leading order (LO), to the momentum fraction $x_+(x_-)$ carried by the parton in the forward-going (backward-going) proton, according to the formula $x_{\pm} = (M_{l\bar{l}}/\sqrt{s})e^{\pm y}$. Therefore, the rapidity and mass distributions are sensitive to the PDFs of the interacting partons. Besides, the transverse momentum p_T distributions of the dilepton provides an additional information about the dynamics of proton collisions at high energy particularly sensitive to the higher-order QCD corrections. In this work, several most recent PDFs parameterizations at the next-to-leading order (NLO) such as MMHT14 [3] and CT14 [4] models, as well as the NLO statistical PDFs previously developed in Ref. [5], will be employed for description of the existing DY data for the differential y , $M_{l\bar{l}}$ and p_T distributions, both at low and high energies. For this purpose, we have selected the data from a limited number of experiments at FNAL Tevatron (E866, D0) and CERN LHC (CMS, ATLAS) keeping only those with the highest integrated luminosity, corresponding to the highest precision.

The paper is organized as follows. In Section 2, we review the main features of three sets of PDFs we have used for our calculations. In Section 3, we consider the invariant mass distribution at LHC (7/8 TeV) energies vs available data over a very broad dilepton mass range up to 2 TeV, and

also in a much smaller mass range from a fixed-target FNAL experiment. In Section 4, the differential cross section as a function of the Z/γ^* rapidity is analyzed. In Section 5, we study the Z/γ^* transverse momentum spectra for two different centre-of-mass energies. We give our final remarks and conclusions in Section 6.

2 PDFs selection

We will now summarize the essential properties of three sets of PDFs which will be tested in our analysis of the DY process.

First, let us recall the main features of the statistical approach [5] for building up the PDFs as opposed to the standard polynomial type parameterizations based on Regge theory at low x and on counting rules at large x . The fermion distributions are given by the sum of two terms, a quasi Fermi-Dirac function and a helicity independent diffractive contribution

$$xq^h(x, Q_0^2) = \frac{A_q X_{0q}^h x^{b_q}}{\exp[(x - X_{0q}^h)/\bar{x}] + 1} + \frac{\tilde{A}_q x^{\tilde{b}_q}}{\exp(x/\bar{x}) + 1}, \quad (1)$$

$$x\bar{q}^h(x, Q_0^2) = \frac{\bar{A}_q (X_{0q}^{-h})^{-1} x^{b_{\bar{q}}}}{\exp[(x + X_{0q}^{-h})/\bar{x}] + 1} + \frac{\tilde{A}_q x^{\tilde{b}_q}}{\exp(x/\bar{x}) + 1}, \quad (2)$$

defined at the input energy scale $Q_0^2 = 1 \text{ GeV}^2$. We note that the diffractive term is absent in the quark helicity distribution Δq and in the quark valence contribution $q - \bar{q}$.

In Eqs. (1) and (2) the multiplicative factors X_{0q}^h and $(X_{0q}^{-h})^{-1}$ in the numerators of the non-diffractive parts of the q 's and \bar{q} 's distributions, imply a modification of the quantum statistical form, which was proposed in order to agree with experimental data ¹. The parameter \bar{x} plays the role of a *universal temperature* and X_{0q}^\pm are the two *thermodynamical potentials* of the quark q , with helicity $h = \pm$. They represent the fundamental characteristics of the model. Notice the change of sign of the potentials and helicity for the antiquarks².

¹These factors were fully justified in the extension of the PDFs to include their transverse momentum dependence (TMD) [6].

²At variance with statistical mechanics where the distributions are expressed in terms of the energy, here one uses x which is clearly the natural variable entering in all the sum rules of the parton model.

Although the statistical approach to the starting PDFs allows the simultaneous description of unpolarized cross sections and helicity asymmetries, a unique situation in the literature, in this work we will restrain ourselves to spin-independent DY observables. For a given flavor q , the corresponding quark and antiquark distributions involve *eight* free parameters: X_{0q}^\pm , A_q , \bar{A}_q , \tilde{A}_q , b_q , \bar{b}_q and \tilde{b}_q . It reduces to *seven* since one of them is fixed by the valence sum rule, $\int (q(x) - \bar{q}(x))dx = N_q$, where $N_q = 2, 1, 0$ for u, d, s , respectively. In the light quark sector $q = \{u, d\}$, the total number of free parameters is reduced to *eight* by applying additional constraints as was done in Ref. [7] (for a more detailed review, see e.g. Ref. [8])

$$A_u = A_d, \quad \bar{A}_u = \bar{A}_d, \quad \tilde{A}_u = \tilde{A}_d, \quad b_u = b_d, \quad \bar{b}_u = \bar{b}_d, \quad \tilde{b}_u = \tilde{b}_d.$$

For the gluon PDF at the input energy scale, we consider the black-body inspired expression

$$xG(x, Q_0^2) = \frac{A_G x^{b_G}}{\exp(x/\bar{x}) - 1}, \quad (3)$$

a quasi Bose-Einstein function, with b_G being the only free parameter, since A_G is determined by the momentum sum rule. To summarize, this determination of all PDF sets³ involves a total of *seventeen* free parameters. Namely, in addition to the temperature \bar{x} and the exponent b_G of the gluon distribution, we have *eight* free parameters for the light quarks (u, d), *seven* free parameters for the strange quarks as was outlined above. These parameters were determined in Ref. [5], from a NLO QCD fit of a large set of accurate DIS data *only*. The resulting PDFs, denoted from now on as BS15, are illustrated for the energy scale $Q^2 = 10 \text{ GeV}^2$ in Fig. 1.

Next we consider an improved version of the so-called MSTW framework which was proposed seven years ago in Ref. [9]. The main shortcoming of the MSTW PDFs was an incorrect description of the lepton charge asymmetry from W^\pm decays as a function of the lepton rapidity. The new input distributions result from major changes in the theoretical procedure with respect to original Ref. [9] since they involve Chebyshev polynomials. In this new version proposed in Ref. [3] the majority of the starting PDFs have the following form

$$xf(x, Q_0^2) = A(1-x)^\eta x^\delta \left[1 + \sum_{i=1}^n a_i T_i^{Ch}(y(x)) \right], \quad (4)$$

³In Ref. [5] we have considered the helicity gluon distribution which is irrelevant in the present work

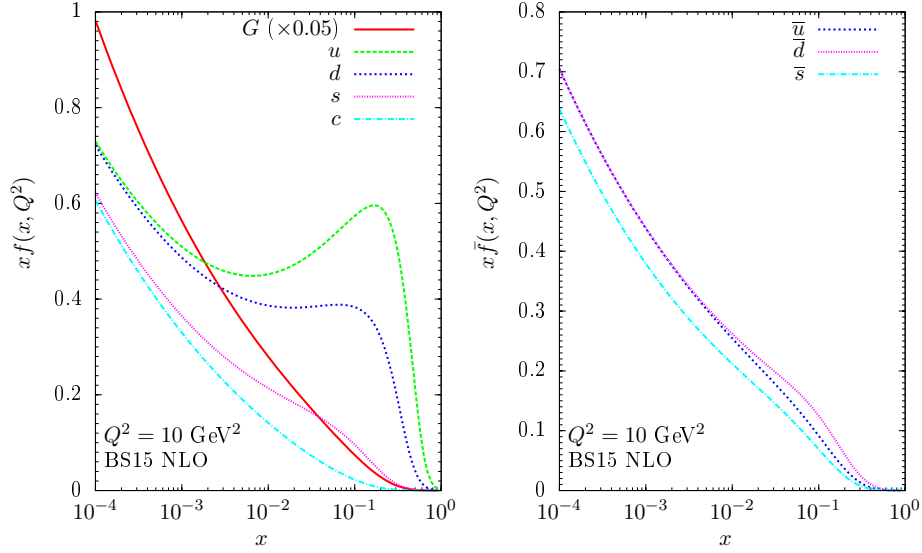


Figure 1: The BS15 PDFs for quarks, gluon (*left*) and antiquarks (*right*) from Ref. [5] at $Q^2 = 10 \text{ GeV}^2$.

where $Q_0^2 = 1 \text{ GeV}^2$ is the input energy scale, and $T_i^{Ch}(y)$ are Chebyshev polynomials in y , with $y = 1 - 2\sqrt{x}$, where one takes $n = 4$. For each PDF, namely, $f = u_V, d_V, S, s_+$ one has to determine the parameters A, η, δ, a_i . Here, u_V and d_V denote the light-quark valence distributions and $S \equiv 2(\bar{u} + \bar{d}) + s_+$ is the light-quark sea distribution. For $s_+ \equiv s + \bar{s}$ one sets $\delta_+ = \delta_S$.

We still have to specify the parameterisations of the gluon and of the differences $\Delta \equiv \bar{d} - \bar{u}$ and $s - \bar{s}$. For Δ one sets $\eta_\Delta = \eta_S + 2$ and one uses the following expression

$$x\Delta(x, Q_0^2) = A_\Delta(1-x)^{\eta_\Delta} x^{\delta_\Delta} (1 + \gamma_\Delta x + \epsilon_\Delta x^2) . \quad (5)$$

For the poorly determined strange quark difference one takes

$$s_- \equiv x(s - \bar{s}) = A_-(1-x)^{\eta_-} x^{\delta_-} (1 - x/x_0) . \quad (6)$$

Finally, for the gluon distribution, as proposed long time ago [10], one needs a second term for the small x behavior as shown below

$$xG(x, Q_0^2) = A_G(1-x)^{\eta_G} x^{\delta_G} \left[1 + \sum_{i=1}^2 a_{G,i} T_i^{Ch}(y(x)) \right] + A_{G'}(1-x)^{\eta_{G'}} x^{\delta_{G'}} , \quad (7)$$

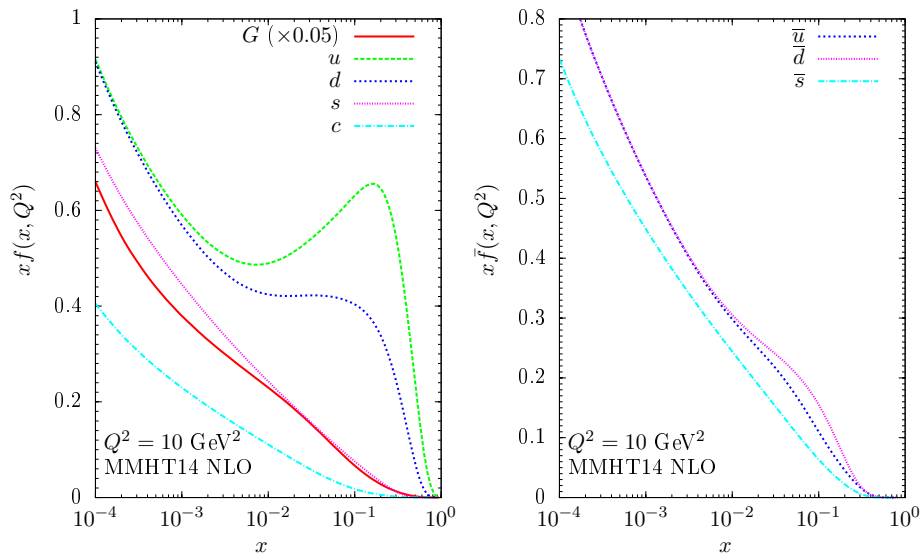


Figure 2: The MMHT14 PDFs for quarks, gluon (*left*) and antiquarks (*right*) from Ref. [3] at $Q^2 = 10 \text{ GeV}^2$.

and we notice that it involves *seven* free parameters since A_G is constrained by the momentum sum rule. This is a major difference with respect to the statistical approach. In total, there are *thirty seven* free parameters, a large number, while one should remember that there are three constraints from the valence sum rules as already mentioned above. In addition, there is also the strong coupling defined at the mass scale of the Z boson, i.e. $\alpha_s(M_Z^2)$, which is allowed to be free when determining the best fit. The authors claim that the advantage of using a parameterisation based on Chebyshev polynomials is the stability and a good convergence of the values found for the coefficients a_i . In what follows, we refer to these PDFs as to the MMHT14 NLO model.

The parameters were determined from a global analysis of a variety of new data sets, from the LHC including some DY results, updated Tevatron data and HERA combined H1 and ZEUS data on the total and charm structure functions. For DIS data on deuterium targets deuteron corrections were taken into account, as well as nuclear corrections for neutrino data. The NLO and a next-to-next-to-leading order (NNLO) QCD fits of the data were performed and we display the resulting PDFs in Fig. 2 at the same energy

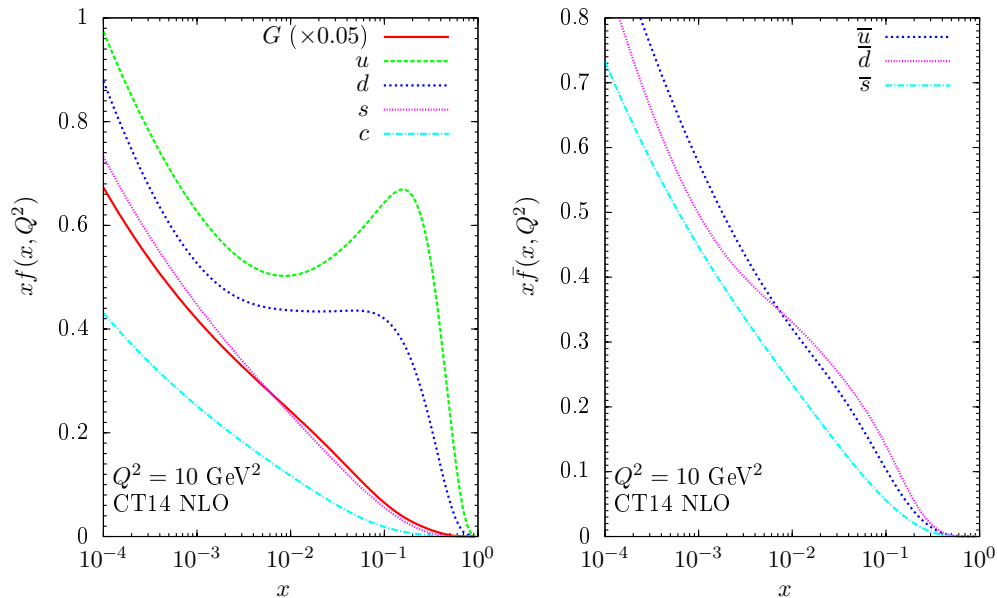


Figure 3: The CT14 PDFs for quarks, gluon (*left*) and antiquarks (*right*) from Ref. [4] at $Q^2 = 10 \text{ GeV}^2$.

scale $Q^2 = 10 \text{ GeV}^2$ as in Fig. 1. The fit quality and the determination of the PDF uncertainties were carefully studied in Ref. [3]. It is interesting to observe that in most cases the new MMHT PDFs are within one standard deviation from those of the MSTW framework [9], a remarkable stability of the procedure.

We now turn to the third PDF set we will use in our calculations of the DY cross sections. It results from different versions [11] up to NNLO, from the CTEQ-TEA global analysis of QCD, including the use of data from HERA, Tevatron and LHC. New theoretical developments are associated to the achievement of an increasing data precision in DIS, vector boson production and single-jet production. It is interesting to note that DY data from colliders were not considered so far. Standard parametrizations for each flavor are of the form

$$x f_a(x, Q_0^2) = x^{a_1} (1-x)^{a_2} P_a(x), \quad (8)$$

where the first two factors are suggested by the Regge theory and by counting rules, and the remaining factor $P_a(x)$ is assumed to be slowly varying. In the

previous CTEQ analyses, $P_a(x)$ for each flavor was chosen as an exponential of a polynomial in x or \sqrt{x} , for instance,

$$P_{q_v}(x) = \exp(a_0 + a_3\sqrt{x} + a_4x + a_5x^2), \quad (9)$$

for valence quarks q_v .

In their most recent work referred to as CT14 [4], for the valence quarks they re-express the polynomial as a linear combination of *Bernstein polynomials* in $y = \sqrt{x}$

$$P_{q_v} = d_0p_0(y) + d_1p_1(y) + d_2p_2(y) + d_3p_3(y) + d_4p_4(y), \quad (10)$$

where $p_0(y) = (1 - y)^4$, $p_1(y) = 4y(1 - y)^3$, $p_2(y) = 6y^2(1 - y)^2$, $p_3(y) = 4y^3(1 - y)$ and $p_4(y) = y^4$. Then seven parameters for each flavor are reduced to just four by setting $d_1 = 1$, $d_3 = 1 + a_1/2$ and using the valence sum rule. So the valence quark u_v and d_v are determined in terms of a total of *eight* free parameters.

The CT14 model uses a similar parameterisation for the gluon but with a polynomial of a lower order since the data provide fewer constraints on the gluon distribution

$$P_g(y) = g_0 [e_0q_0(y) + e_1q_1(y) + q_2(y)], \quad (11)$$

where $q_0(y) = (1 - y)^2$, $q_1(y) = 2y(1 - y)$, and $q_2(y) = y^2$. However, instead of $y = \sqrt{x}$, it employs $y = 1 - (1 - \sqrt{x})^2 = 2\sqrt{x} - x$. The momentum sum rule reduces the total number of parameters of the gluon distributions down to *five*. The sea quark distributions \bar{d} and \bar{u} were parametrized using fourth-order polynomials in y with the same variable $y = 2\sqrt{x} - x$ that was used for the gluon. They assumed $\bar{u}(x)/\bar{d}(x) \rightarrow 1$ at $x \rightarrow 0$, which implies $a_1(\bar{u}) = a_1(\bar{d})$.

All in all, the CT14 model has *eight* free parameters associated with the valence quarks, *five* parameters associated with the gluon, and *thirteen* parameters associated with sea quarks, which in total amounts to *twenty six* fitting parameters. The initial energy scale $Q_0=1.295$ GeV has been used to perform the NLO and NNLO QCD fits of a large set of data. We display the resulting PDFs in Fig. 3 at $Q^2 = 10$ GeV² as a reference.

All the PDFs considered in this work were obtained from their correspondent LHAPDF6 [12] grids, which were used in our Monte-Carlo simulations described below⁴.

⁴The LHADPF grids for the BS15 NLO model shall appear in online database soon.

3 Dilepton invariant mass distribution

Consider first, as displayed in Fig. 4, the measurement of DY cross section at the LHC energy 8 TeV allowing to get dilepton mass up to 2 TeV. The

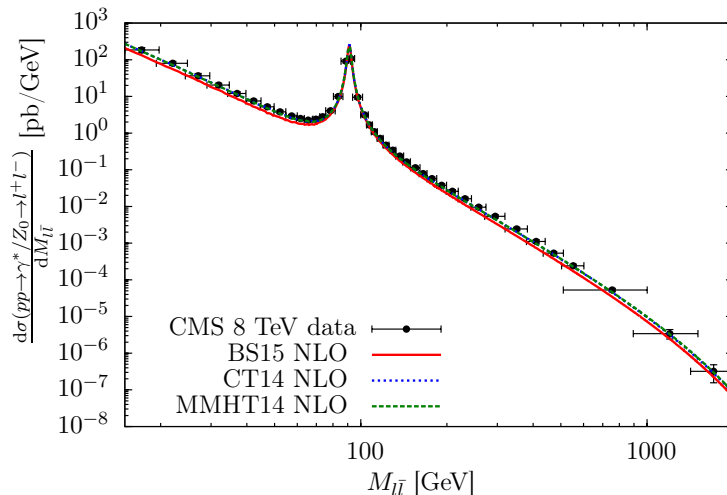


Figure 4: The DY differential cross section measured in the combined di-muon and di-electron channels by CMS at $\sqrt{s} = 8$ TeV over the invariant mass range from 15 GeV to 2 TeV [13] vs QCD NLO predictions obtained by using PDF models from Refs. [3, 4, 5].

NLO cross section at LHC energies was calculated using the q_T subtraction method implemented in the DYNNLO code [14]. This semi-analytical tool employs the dipole subtraction formalism of Catani and Seymour [15] realised by using the MCFM event generator [16] and stands as one of the up-to-date calculations of the Drell-Yan process up to NNLO. In the case of the invariant mass distributions the full phase space is integrated within each bin in the dilepton mass $M_{l\bar{l}}$. Note, in all the calculations here and below the factorisation and renormalisation scale are taken to be equal to the transverse mass of the dilepton pair, by convention. One notices that the theoretical results with distinct PDFs behave similarly for a broad range of the invariant mass with minor differences.

The DY low mass region was specifically measured by the ATLAS Collaboration at luminosities of 1.6 fb^{-1} and 35 pb^{-1} [17], for which a comparison with three distinct NLO PDFs based on the DYNNLO implementation is

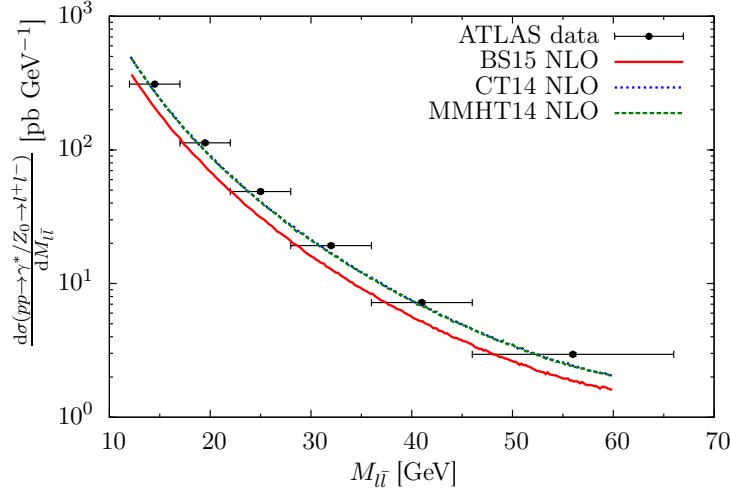


Figure 5: The DY differential cross section measured in the combined di-muon and di-electron channels by ATLAS at $\sqrt{s} = 7$ TeV over the extended mass range 12 – 66 GeV [17] vs QCD NLO predictions obtained by using PDF models from Refs. [3, 4, 5].

shown in Fig. 5. The data used the invariant mass region of 26 – 66 GeV for the higher luminosity whereas less precise data extend this region down to 12 GeV. Here, one starts to observe a minor deviation between predictions of BS15 and the other two PDFs. While the results of MHHT and CT models are closer to data, the BS15 predictions are still within the experimental error bars.

We also selected the data for the high mass DY electron-positron pair production measured by the ATLAS Collaboration [18] which correspond to 4.9 fb^{-1} luminosity within the mass range of $116 < M_{e^+e^-} < 1500$ GeV and in the kinematics defined by di-electron pairs with $p_{\perp} > 25$ GeV and $|\eta| < 2.5$. In Fig. 6 the high mass distribution of e^+e^- pairs is compared with the corresponding NLO pQCD predictions. The CT14 and MMHT14 results are pretty close to each other and show a very good agreement with data, while the BS15 result is somewhat below the data but is still within the error bars.

At much lower energies at FNAL $\sqrt{s} = 38.8$ GeV the E866/NuSea Collaboration provided the DY differential distributions over a broad kinematics range [20]. In this case, we have implemented the formalism by Sutton et

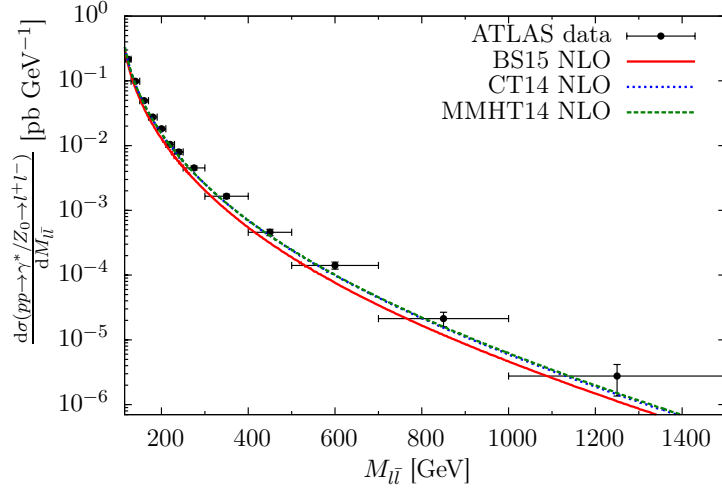


Figure 6: The DY differential cross section measured in the di-electron channel by ATLAS at $\sqrt{s} = 7$ TeV over the high-mass range 116 – 1500 GeV [18] vs QCD NLO predictions obtained by using PDF models from Refs. [3, 4, 5].

al. [19] where both NLO corrections for Compton and annihilation subprocesses were included. This formalism results in a fair description of the E866/NuSea data on DY differential distributions in the proton-proton collisions for three PDF models (BS15, CT14 and MMHT14) at various $\langle x_F \rangle$ and dilepton masses shown in Fig. 7. Here, an overall uncertainty w.r.t. scale variations within the interval $M_{l\bar{l}}/2 < \mu < 2M_{l\bar{l}}$ is shown as filled error bands. Note, the uncertainties grow with $\langle x_F \rangle$ similarly in all three models. Noticeable deviations between the predictions from distinct PDF sets emerge mostly at small invariant masses $M_{l\bar{l}} < 6$ GeV where some deficiency of the predictions can be observed. Specifically for this case, one observes that the CT14 PDF is rather unstable at $\langle x_F \rangle = 0.075$ and the CT14/BS15 PDFs do not work well at $\langle x_F \rangle \simeq 0.5 - 0.7$, while MMHT14 demonstrates a better description in both normalisation and shape. For intermediate values of the Feynman variable and large $M_{l\bar{l}}$ all the considered PDFs provide a fairly good description of the low energy data.

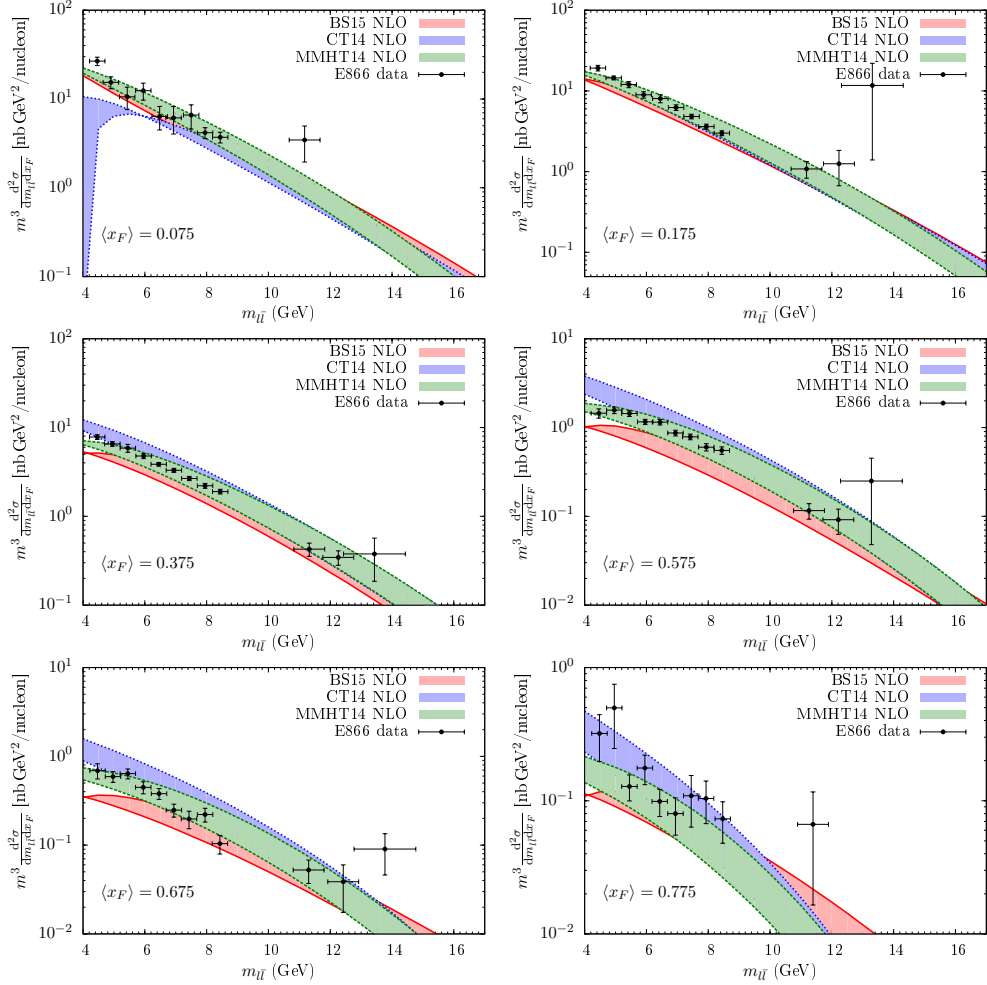


Figure 7: The DY differential cross section measured in the di-muon channel by the E866 Collaboration at $\sqrt{s} = 38.8$ GeV [20] over a low-mass range and various Feynman $\langle x_F \rangle$ variables vs QCD NLO predictions obtained by using PDF models from Refs. [3, 4, 5]. The uncertainty w.r.t. scale variations within the interval $M_{lil}/2 < \mu < 2M_{lil}$ is shown as filled error bands.

4 Z/γ^* boson rapidity distribution

The events and analyses for this and further sections were generated with Pythia v8 [21] and Rivet [22]. For the Z/γ^* boson rapidity distribution the standard LO Pythia (with parton showers and NLO PDFs) was employed.

The parton shower within Pythia effectively resums the higher-order real corrections due to emissions off the colored initial states. The latter corrections significantly affect the kinematics of the final states and is need for a proper treatment of the differential distributions. Therefore, this approach differs from the full NLO calculation by the virtual corrections only. However, these corrections can only affect the overall normalisation of the cross sections and are typically accounted for by a universal K -factor which is practically independent on kinematics of the final states. Since the experimental data for the Drell-Yan process at Tevatron and LHC are typically provided in terms of ratios of the differential-to-total cross sections, one does not need to explicitly compute the virtual corrections since they cancel out in these ratios and do not affect our conclusions. Besides, other model uncertainties such as the scale uncertainty mostly cancel in such ratios as well. So it is not surprising that this method leads to a very good agreement of various PDF models with the Tevatron and LHC data on the ratios in the whole kinematic region (see below).

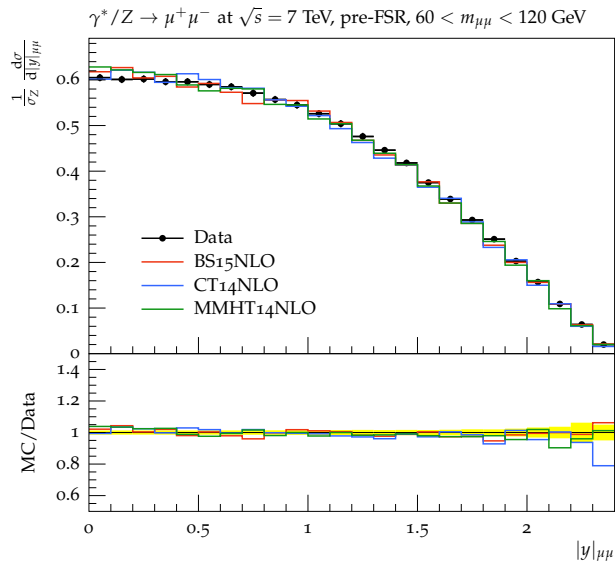


Figure 8: The DY differential cross section measured in the di-muon channel by CMS at $\sqrt{s} = 7$ TeV [23] vs QCD NLO predictions obtained by using PDF models from Refs. [3, 4, 5].

For validation of the considered PDF models and theoretical methods,

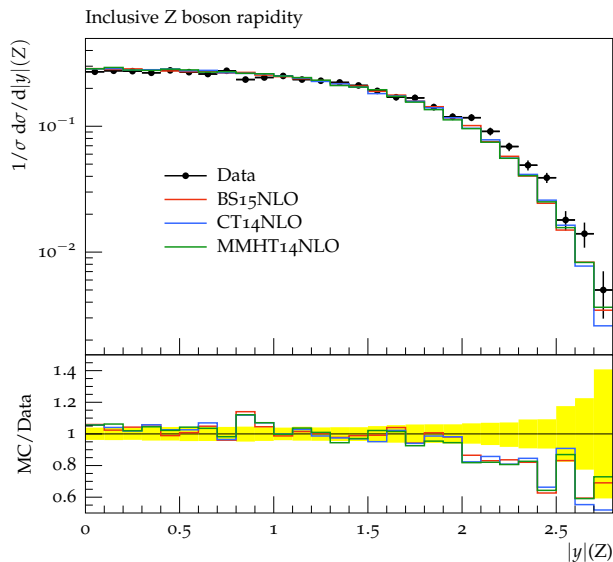


Figure 9: The DY differential cross section measured in the di-electron channel by the D0 Collaboration at $\sqrt{s} = 1.96$ TeV [24] vs QCD NLO predictions obtained by using PDF models from Refs. [3, 4, 5].

we display in Fig. 8 the results on the rapidity distribution from the CMS Collaboration at $\sqrt{s} = 7$ TeV [23] corresponding to the integrated luminosity of $4.5(4.8) \text{ fb}^{-1}$. The di-muon channel was used for rapidity reconstruction within certain invariant mass intervals, from which we have selected the one corresponding to a vicinity of the Z peak, $60 < m_{\mu\bar{\mu}} < 120$ GeV. Analogously, the rapidity distributions from the D0 Collaboration at a lower energy $\sqrt{s} = 1.96$ TeV [24] in the di-electron channel and the mass range $71 \leq M_{e^+e^-} \leq 111$ GeV corresponding to an integrated luminosity of 0.4 fb^{-1} were compared to the theoretical predictions with BS, MHHT and CT models. The corresponding results are shown in Fig. 9. All the NLO pQCD predictions exhibit a fair agreement with the existing data from both LHC and Tevatron measurements.

5 Z/γ^* boson transverse momentum spectrum

A high-precision data on the Z/γ^* boson transverse momentum distribution up to 800 GeV has been presented by ATLAS in Ref. [25] at $\sqrt{s} = 7$ TeV cor-

responding to the integrated luminosity of 4.7 fb^{-1} . In Fig. 10 we consider the full detector acceptance whereas the Z -boson transverse momentum for three different rapidity bins is shown in Fig. 11. A good description was obtained as well including rather high- p_{\perp} region where in principle the higher order corrections could start to play an important role, as well as the statistical fluctuations for the forward region ($2 < |y_Z| < 2.4$) could become noticeable due to a smaller number of events generated in the forward/high- p_T kinematics. A disagreement of the model predictions in the highest p_{\perp} bins, besides poor statistics, could be due to the fact we employ the simplistic analysis with LO matrix elements and NLO PDFs (plus parton shower) and not the full-precision higher-order $Z + jets$ matrix elements. Remarkably enough, one can see that the PDFs tested here and our simplistic LO analysis give a fair description of data for almost entire range of Z -boson p_T 's.

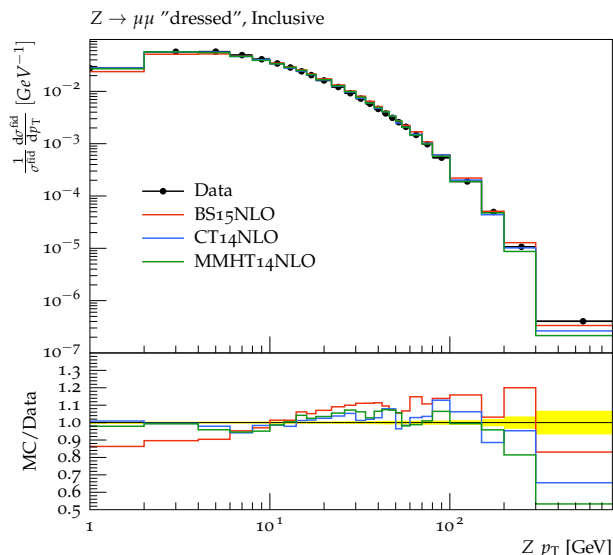


Figure 10: The ATLAS 7 TeV data on Z -boson transverse momentum distribution with the full detector acceptance [25] vs QCD NLO predictions obtained by using PDF models from Refs. [3, 4, 5].

It is worth to present similar results for the Z/γ^* boson transverse momentum distribution from the D0 Collaboration at Tevatron [26] in $p\bar{p}$ collisions at $\sqrt{s} = 1.96 \text{ TeV}$ in the di-electron channel corresponding to the integrated luminosity of 0.98 fb^{-1} . In Fig. 12 the Z -boson transverse momentum distribution is plotted in two regions, the one that covers the full detector ac-

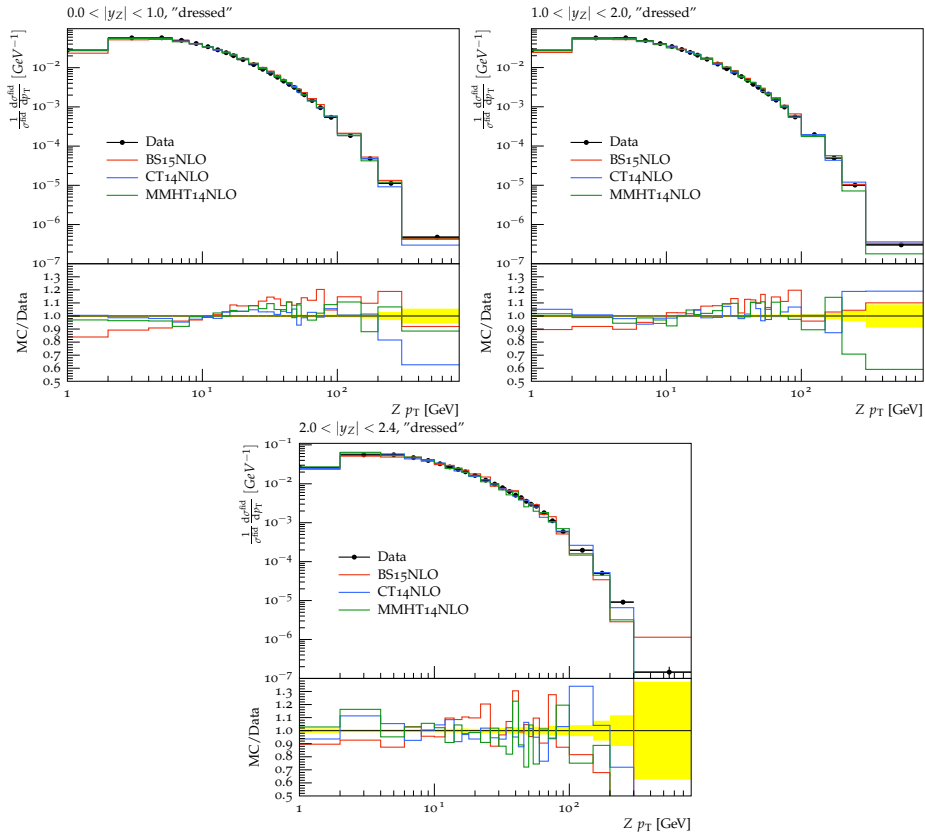


Figure 11: The ATLAS 7 TeV data on Z -boson transverse momentum distribution for three different rapidity bins [25] vs QCD NLO predictions obtained by using PDF models from Refs. [3, 4, 5].

ceptance and the one which is focused on forward production, *i.e.*, for $\eta > 2$ and $p_{\perp} < 30$ GeV. Similarly to the LHC case, the theoretical modelling with the chosen PDFs exhibit rather good description of the Tevatron data within the experimental uncertainties.

6 Concluding remarks

To summarize, the NLO pQCD predictions with the MHHT14, CT14 and BS15 PDFs studied in this work have resulted in a fair description of a broad range of DY data from FNAL-NUSEA energies up to LHC energies while

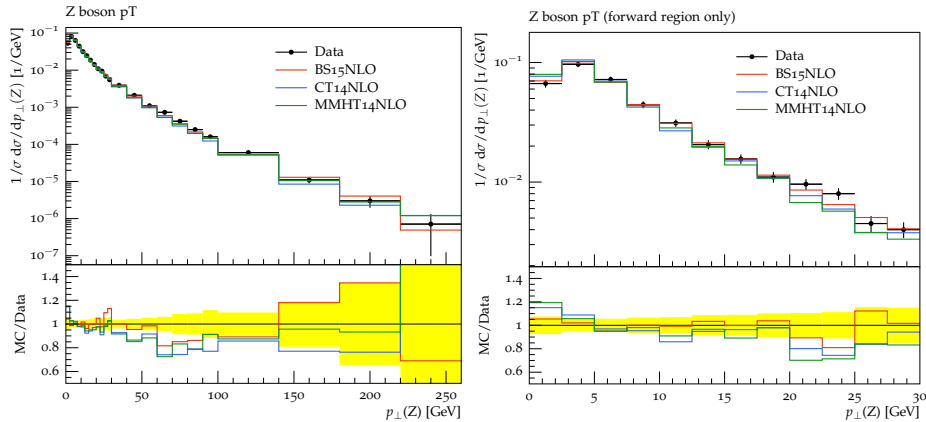


Figure 12: Data from D0 [26] at 1.98 TeV on Z -boson transverse momentum distribution for two kinematic regions vs QCD NLO predictions obtained by using PDF models from Refs. [3, 4, 5].

a few minor deviations, mainly at the edges of the respective phase space, have been observed. Given the fact that three very different PDF sets lead to rather similar results we conclude that the NLO BS15 model having a much fewer free parameters which are fitted to the DIS data only is not worse than the other most recent parameterisations and should be considered on the same footing as the current global PDF fits when it comes to the DY process at high energies.

Extrapolating to the Drell-Yan process at even larger energies of LHC Run II ($\sqrt{s} = 13$ TeV) we do not expect more significant differences between the BS15 predictions and those of other PDF models since typical x values we probe there get even smaller at higher energies. In Fig. 13 we present (anti)quark PDF CT14-to-BS15 ratios (central values) as functions of x and $Q^2 = 1, 10, 100$ GeV². This figure demonstrates that the differences between the considered PDFs becomes smaller at larger Q^2 and $x \lesssim 10^{-2}$ typical for Drell-Yan at large $M_{\bar{l}l}$ at the LHC; inclusion of error bars does not change this picture. Similar situation holds for comparison of BS15 with the MHHT14 PDFs. As an illustration, in Fig. 14 (left) we show the transverse momentum distributions of the Z -boson at $\sqrt{s} = 13$ TeV for BS15, CT14 and MHHT14 PDFs. A noticeable deviation of the BS15 prediction, which lies below the other PDFs, is seen only at low $p_{\perp}^Z < 10$ GeV, otherwise differences between the predictions for this and other observables such as y and $M_{\bar{l}l}$ distributions

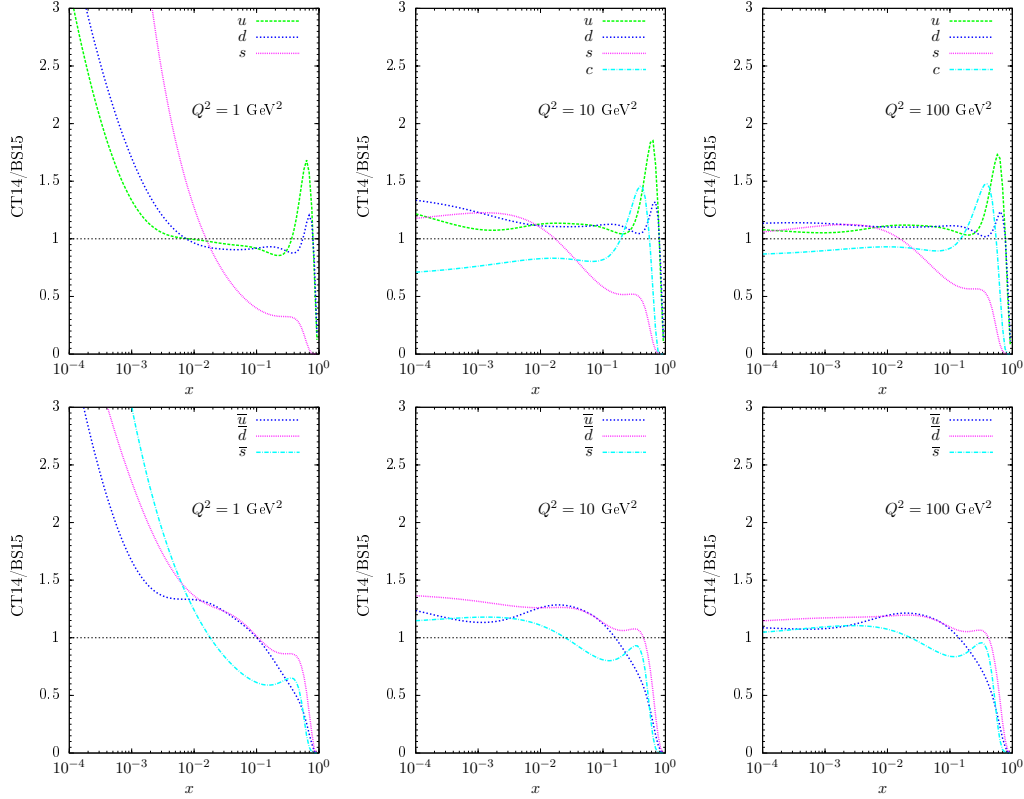


Figure 13: The CT14-to-BS15 ratios for quark (upper row) and antiquark (lower row) NLO PDFs as functions of x and $Q^2 = 1, 10, 100 \text{ GeV}^2$.

are small. We conclude that the BS15 NLO PDF is a good tool to investigate pQCD physics in the second run of LHC measurements.

As is seen in Fig. 7, at low energies the PDF models exhibit more substantial differences in shapes of the invariant mass and x_F distributions than those at high energies. This fact indicates the critical importance of low energy Drell-Yan measurements such as the FNAL E906/SeaQuest experiment [27]. In particular, the E906 experiment will determine the ratio \bar{d}/\bar{u} at large x (up to $x \sim 0.5 - 0.6$). The statistical BS15 model predicts $\bar{d}/\bar{u} > 1$ at large x as illustrated in Fig. 14 (right) together with CT14 and MMHT14 predictions where the filled bands correspond to scale variations within $1 < Q^2 < 100 \text{ GeV}^2$ interval for each PDF model. This characteristic effect is based on the Pauli exclusion principle and the fact that in the proton there are two

u -quarks and one d -quark such that more \bar{d} compared to \bar{u} . A high precision measurement of such a ratio would therefore become a crucial test of physics behind the PDF models.

Acknowledgments

Useful discussions with Gunnar Ingelman, Jesper Roy Christiansen and Torbjorn Sjöstrand are gratefully acknowledged. E. B. is funded by CAPES and CNPq (Brazil), contract numbers 2362/13-9 and 150674/2015-5. R. P. is supported by the Swedish Research Council, contract number 621-2013-428.

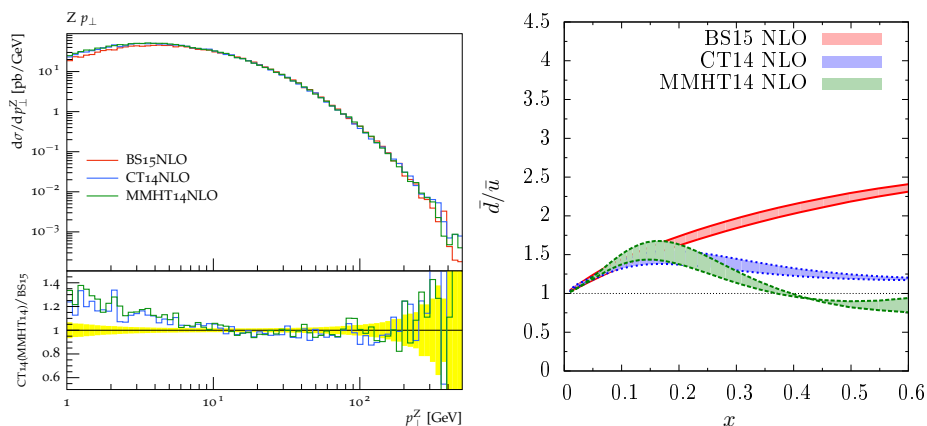


Figure 14: Predictions for the Z boson transverse momentum distribution at $\sqrt{s} = 13$ TeV (left panel) and for the ratio of sea quark PDFs \bar{d}/\bar{u} as a function of fraction x with scale variations within $1 < Q^2 < 100$ GeV² interval (right panel) obtained by using PDF models from Refs. [3, 4, 5].

References

- [1] S. D. Drell and T.-M. Yan, Phys. Rev. Lett. **25**, 316 (1970); Ann. Physics **66**, 578 (1971).
- [2] J. C. Peng and J. W. Qiu, Prog. Part. Nucl. Phys. **76**, 43 (2014).
- [3] L. A. Harland-Lang, A. D. Martin, P. Motylinsky and R. S. Thorne, Eur. Phys. J. **75** 5, 204 (2015).
- [4] S. Dulat *et al.*, arXiv:1506.07443v2 [hep-ph].

- [5] C. Bourrely and J. Soffer, Nucl. Phys. A **941**, 307 (2015).
- [6] C. Bourrely, F. Buccella and J. Soffer, Int. J. Mod. Phys. A **28**, 1350026 (2013).
- [7] C. Bourrely, F. Buccella and J. Soffer, Eur. Phys. J. C **23**, 487 (2002).
- [8] C. Bourrely, J. Soffer and F. Buccella, Eur. Phys. J. C **41**, 327 (2005).
- [9] A. D. Martin, W. J. Stirling, R. S. Thorne and G. Watt, Eur. Phys. J. **63**, 189 (2009).
- [10] A. D. Martin, R. Roberts, W. J. Stirling and R. S. Thorne, Eur. Phys. J. **23**, 73 (2002).
- [11] P. M. Nadolski *et al.*, Phys. Rev. D **78**, 013004 (2008);
J. Pumplin *et al.*, Phys. Rev. D **80**, 014019 (2009);
H. -L. Lai *et al.*, Phys. Rev. D **82**, 074024 (2010).
- [12] A. Buckley *et al.*, Eur. Phys. J. C **75** 132 (2015).
- [13] V. Khachatryan *et al.* (CMS Collaboration), Eur. Phys. J. **75**, 147 (2015).
- [14] S. Catani, L. Cieri, G. Ferrera, D. de Florian, M. Grazzini, Phys. Rev. Lett. **103** 082001 (2009);
S. Catani, M. Grazzini, Phys. Rev. Lett. **98** 222002 (2007).
- [15] S. Catani and M. H. Seymour, Phys. Lett. B **378** (1996) 287;
Nucl. Phys. B **485** (1997) 291 [Erratum-ibid. B 510 (1998) 503].
- [16] J. Campbell, R.K. Ellis, *MCFM - Monte Carlo for FeMtobarn processes*, <http://mcfm.fnal.gov>.
- [17] G. Aad *et al.* (ATLAS Collaboration), JHEP **1406**, 112 (2014).
- [18] G. Aad *et al.* (ATLAS Collaboration), Phys. Lett. B **725** 223 (2013).
- [19] P. J. Sutton, A. D. Martin, R. G. Roberts and W. J. Stirling, Phys. Rev. D **45**, 2349 (1992).
- [20] J. C. Webb *et al.* (FNAL E866/NuSea Collaboration), arXiv:hep-ex/0302019; arXiv:hep-ex/0301031.

- [21] T. Sjöstrand *et al.*, Comput. Phys. Commun. **191**, 159 (2015).
- [22] A. Buckley *et al.*, Comput. Phys. Commun. **184**, 2803 (2013).
- [23] S. Chatrchyan *et al.* (CMS Collaboration), JHEP **1312**, 030 (2013).
- [24] V. Abazov *et al.* (D0 Collaboration), Phys. Rev. D **76**, 012003 (2007).
- [25] G. Aad *et al.* (ATLAS Collaboration), JHEP **1409**, 145 (2014).
- [26] V. Abazov *et al.* (D0 Collaboration), Phys. Rev. Lett. **100**, 102002 (2008).
- [27] P. E. Reimer [Fermilab SeaQuest Collaboration], J. Phys. Conf. Ser. **295**, 012011 (2011).